International Journal of Engineering Science Invention
ISSN (Online): 2319 – 6734, ISSN (Print): 2319 – 6726
www.ijesi.org Volume 2 Issue 7 ǁ July. 2013 ǁ PP.05-16

Dynamic analysis of remotely operated underwater vehicle model

A. M. Badawy [1], A.A.Omer[2]
[1](Mechanical Engineering Department, Military Technical College. / Cairo, Egypt.)
[2](Mechanical Engineering Department, Military Technical College / Cairo, Egypt.)

ABSTRACT: *Dynamic analyses of submerged structures, especially Remotely Operated Underwater Vehicles (ROV) are the first step to build and design an underwater vehicle. In the present paper, the dynamic analysis introduces the equation of motion representing the dynamic behavior of the vehicle under the effect of the hydrodynamic loads. Equations represent the added mass coefficients are used mathematically to estimate the added mass coefficients. The added mass coefficients are estimated also experimentally by means of a free decay pendulum motion test. The hydrodynamic coefficients (linear and quadric damping coefficients) are determined using the computational fluid dynamic through software ANSIS CFX. These coefficients are compared by the coefficients estimated experimentally by means of a free decay pendulum motion test. Good agreement between practical and CFD hydrodynamic coefficient is achieved. The variation of ROV acceleration and velocity with time is obtained for surge and heave directions with varying thrusting load.*

KEYWORDS: *Finite element method; Computational Fluid Dynamic CFD; Hydrodynamic coefficient; added mass; surge; heave.*

I. INTRODUCTION

ROV's are one of the systems used to explore the underwater environment, the extreme underwater environment which needed to be explored and controlled obligate the designer to create a system capable of withstanding these conditions. The high pressure produced from the water column weight plus the dynamic pressure produced from the vehicle speed has to be considered. In order to simulate the motion of underwater vehicle as near to real as possible a good, accurate, and more or less simple modeling should be presented. Several authors [1-5] used two orthogonal coordinate systems to establish a dynamic model, one is a global coordinate system (O,X,Y,Z) fixed at the ocean surface ship with origin at O, Z axis pointing vertically down to the water, and the X,Y axes being in two mutually perpendicular horizontal directions. The other is local coordinate system (o,x,y,z) fixed on the vehicle with the origin at o, x axis pointing to the nose of the vehicle, z axis pointing to the belly of the vehicle and the y axis completing the right-hand system with the other two axis.

Thrusters are the source of the propulsion force moving the vehicle; also represent the force vector in the equation of motion, which decide the way the vehicle moves or respond. Thrusters also had great keenness from authors [1-5]; they consider the thruster force and moment as a constant value regardless the ambient flow. But Jinhyun K., Wan K. C. [6] studied the effect of ambient flow on the thruster. Total mass matrix of the remotely operated vehicle was presented by ZHU Ke-qiang et. al. [5] who said that all vehicles have a longitudinal symmetric plane xoz (yG=0), the added mass coefficients Aij with (i+j) odd are all zeros. The total mass matrix [M] consisting of inertia and added mass terms. Modeling of the coupled motion of the structure and the fluid also is of great effect on the motion study and on stress analysis. François A. and Jose A. [7], explained all the issues concerning fluid structure interaction problems (coupled motion, drag force, added mass, hydrodynamic coefficients ...etc).

In the present paper, equations define the added mass coefficients are used mathematically to estimate the added mass coefficients. The added mass coefficients are estimated experimentally by means of a free decay pendulum motion test. The free decay pendulum motion test is used also to determine the linear and quadric damping coefficients which are compared with the linear and quadric damping coefficient estimated by a Computational Fluid Dynamic model using ANSYS CFX®.

It is found that the use of free decay pendulum motion test gives sufficient results for hydrodynamic coefficients. The open frame ROV could be created with low strength materials, since the load is equally distributed over all surfaces preventing the buckling hazard. Good agreement between hydrodynamic coefficients obtained using free decay pendulum motion and the computational fluid dynamics CFX.

II. STRUCTURE DESIGN

The ROV structure mainly made to support the instrumentations and other systems installed on the ROV frame, and keep it safe. It is essential in the field of underwater vehicle design to select the suitable frame, holding the sensors, driving, and control instruments. ROV structure could be open or closed frame according to the operation environment.

2.1 Shape and material selection

The materials have a great contribution on the structure process, underwater conditions obligates the designer to use materials with high corrosion resistance also with high strength to withstand the high pressure especially for high depth ROV's. Aluminum titanium alloys are widely used in ROV's programs; they have high strength and high corrosion resistance, also with light weight for saving the active energy and to reduce the inertia force produced from the vehicle's acceleration [8]. During this study a PVC open shell frame is used as shown in Fig.1. PVC is used for its low weight, low price, and ease of assembly.

2.2 ROV Frame characteristics

The frame selected is 0.38*0.38*0.18 m parallelogram shape made from one inch PVC tubes. The tubes are pasted using a special paste to prevent any slippage during operation. The tubes are including different holes to permit the water to inter the tubes which insure more stability to the vehicle. The ROV frame used is made of PVC with a density of 1323 kg/m3, total in air weight of 2.557 Kg, while the holes causes the additional water weight of 1.182 kg, this gives a total ROV weight of 3.739 kg. The center of gravity of the frame is located in the middle of the frame due to the similarity of the frame around the three axes. While the same frame has buoyancy force of 2.24 kg force due to volume of the frame submerged in the water of density 1000 kg/m3.
As shown from the values above the total weight is higher than the buoyancy force, which means negative buoyancy of the frame.

Fig. 1 ROV open frame

2.3 Thruster layout configuration

The layout of the thrusters on the frame are controlled by the number of degrees of freedom needed to the vehicle, also the thrusters' layout might be useful in fault accommodation in case of thruster fault. In the present case study the motion needed to be achieved is translation in surge (x), and heave (y), and rotation about (y) yaw motion. For this type of motion 3 thrusters is installed in the location shown in Fig. 2. This configuration support the vehicle with the three degree of freedom motion needed.

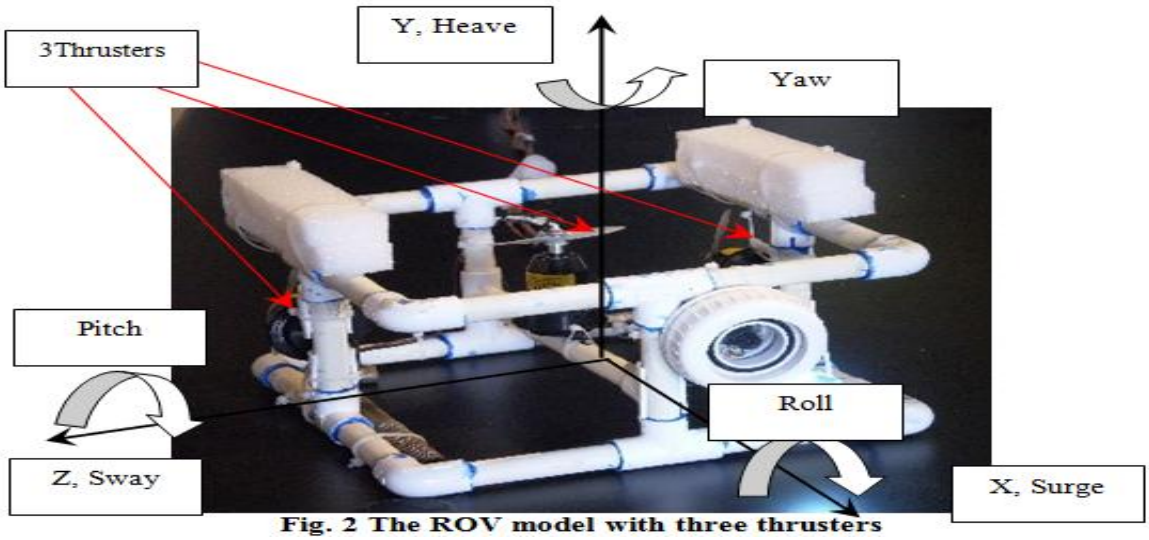

Fig. 2 The ROV model with three thrusters

III. MATHEMATICAL MODEL

In order to dynamically analyze the ROV the following equation of motion is used [9],

$$[M][\ddot{q}] + [M_{added}][\ddot{q}] + [K_l][\dot{q}] + [K_q]|[\dot{q}]|[\dot{q}] = [T] \quad (1)$$

Where $[T]$ Thrusting force vector, $[K_l][\dot{q}]$ linear damping force vector, $[K_q][\dot{q}]^2$ Quadric damping force vector and $[M_{added}][\ddot{q}]$ Added mass inertia force.

3.1 Equivalent mass matrix

For body movies in six degree of freedom (serge, sway, heave, roll, pitch, yaw) a 6x6 mass matrix is presented, and the form.

$$[M] = \begin{bmatrix} m & 0 & 0 & 0 & 0 & 0 \\ 0 & m & 0 & 0 & 0 & 0 \\ 0 & 0 & m & 0 & 0 & 0 \\ 0 & 0 & 0 & I_x & 0 & 0 \\ 0 & 0 & 0 & 0 & I_y & 0 \\ 0 & 0 & 0 & 0 & 0 & I_z \end{bmatrix}$$

The ROV model shown in Fig.1 is consists of 8 tubes each of length 0.38 meter and 0.0125 m radius, and 4 tubes of length 0.18 meters and 0.0125 meters radius. The tubes centeroidal mass moments of inertia are calculated and the shift theorem is applied. The summation is presented to get the mass moment of inertia of the total structure. The frame is assumed to be filled with water. The frame material density ρ is 1323 kg/m^3 and water density of 1000 kg/m^3. For each tube of length L, radius R, the mass moment of inertia is calculated, where I_x, I_y and I_z are local moment of inertia, and $I_x^{/}$,$I_y^{/}$ *and* $I_z^{/}$ are total mass moment of inertia with respect to the center of the structure, m is the total mass of the tubes that field with water. The values of mass and mass moment of inertia are summarized in Table (1), where $I_x^{/} = I_z^{/}$ due to symmetry.

Table1 Numerical values of mass and mass moment of inertia

Variable	Value
m	3.739 Kg
$I_{x'}$	0.097 Kg. m^2
$I_{y'}$	0.154 Kg. m^2
$I_{z'}$	0.097 Kg. m^2

Substituting the obtained values of total mass and mass moment of inertia into the mass matrix gives the following mass matrix:

$$[M] = \begin{bmatrix} 3.739 & 0 & 0 & 0 & 0 & 0 \\ 0 & 3.739 & 0 & 0 & 0 & 0 \\ 0 & 0 & 3.739 & 0 & 0 & 0 \\ 0 & 0 & 0 & 0.097 & 0 & 0 \\ 0 & 0 & 0 & 0 & 0.154 & 0 \\ 0 & 0 & 0 & 0 & 0 & 0.097 \end{bmatrix}$$

3.2 Added mass

When a rigid body is moving in a fluid, the additional inertia of the fluid surrounding the body, which is accelerated by the movement of the body, has to be considered. The fluid surrounding the body is accelerated with the body itself, a force is then necessary to achieve this acceleration; the fluid exerts a reaction force which is equal in magnitude and opposite in direction. This reaction force is the added mass contribution. Gianluca Antonelli [12] divided the added mass matrix into two matrices M_A and C_A can therefore be considered:

$M_A = -\text{diag.}\ \{X_{\dot{u}}, Y_{\dot{v}}, Z_{\dot{w}}, K_{\dot{p}}, M_{\dot{q}}, N_{\dot{r}}\}$ (2)

$$C_A = \begin{bmatrix} 0 & 0 & 0 & 0 & -Z_{\dot{W}} w & Y_{\dot{V}} v \\ 0 & 0 & 0 & Z_{\dot{W}} w & 0 & -X_{\dot{U}} u \\ 0 & 0 & 0 & -Y_{\dot{V}} v & X_{\dot{U}} u & 0 \\ 0 & -Z_{\dot{W}} w & Y_{\dot{V}} v & 0 & -N_{\dot{r}} r & M_{\dot{q}} q \\ Z_{\dot{W}} w & 0 & -X_{\dot{U}} u & N_{\dot{r}} r & 0 & -K_{\dot{p}} p \\ -Y_{\dot{V}} v & X_{\dot{U}} u & 0 & -M_{\dot{q}} q & -K_{\dot{p}} p & 0 \end{bmatrix} \quad (3)$$

The added mass coefficients can be theoretically derived by exploiting the geometry of the rigid body and, eventually, its symmetry, by applying the strip theory. For a cylindrical rigid body of mass m_c, length L_c, with circular section of radius r the following added mass coefficients can be derived [12]:

$X_{\dot{u}} = -0.1 m_c$ (4)

$Y_{\dot{v}} = -\pi \rho_c r^2 L_c$ (5)

$Z_{\dot{w}} = -\pi \rho_c r^2 L_c$ (6)

$K_{\dot{p}} = 0$ (7)

$M_{\dot{q}} = -1l12\ \pi \rho_c r^2 L_c$ (8)

$Nr^{\cdot} = -1l12\ \pi \rho_c r^2 L_c$ (9)

where m_c mass of each cylinder filled by water, L_c, length of each cylindrical tube, ρ_c density of each cylinder filled by water .

Substituting in the above equations for each cylinder and make summation for all cylinders leads to the values of the added mass matrix coefficient shown in Table (2).

Table 2 Values of added mass matrix coefficients

Element	Value	
$X_{\dot{u}}$	-0.54403	Kg
$Y_{\dot{v}}$	-1.564	Kg
$Z_{\dot{w}}$	-0.54403	Kg
$K_{\dot{p}}$	-9.93667E-06	$Kg.m^2$
$M_{\dot{q}}$	-1.7964E-05	$Kg.m^2$
$N_{r^{\cdot}}$	-9.93667E-06	$Kg.m^2$

Then, the added mass matrix is: $M_{added} = M_A + C_A$

$$M_{added} = \begin{bmatrix} 0.544 & 0 & 0 & 0 & 0.544w & -1.564v \\ 0 & 1.564 & 0 & -0.544w & 0 & 0.544u \\ 0 & 0 & 0.544 & -1.564v & -0.544u & 0 \\ 0 & 0.544w & -1.564v & 9.94E-6 & 9.94E-6r & -1.79E-5q \\ -0.544w & 0 & 0.544u & -9.94E-6r & 1.76E-5 & 9.94E-6p \\ 1.564v & -0.544u & 0 & 1.79E-5q & -9.94E-6p & 9.94E-6 \end{bmatrix}$$

By substituting into equation 1, the equation of motion of the entire structure will be as follows:-

$$\begin{bmatrix} 3.739 & 0 & 0 & 0 & 0 & 0 \\ 0 & 3.739 & 0 & 0 & 0 & 0 \\ 0 & 0 & 3.739 & 0 & 0 & 0 \\ 0 & 0 & 0 & 0.097 & 0 & 0 \\ 0 & 0 & 0 & 0 & 0.154 & 0 \\ 0 & 0 & 0 & 0 & 0 & 0.097 \end{bmatrix} \begin{bmatrix} \dot{u} \\ \dot{v} \\ \dot{w} \\ \dot{p} \\ \dot{q} \\ \dot{r} \end{bmatrix} +$$

$$\begin{bmatrix} 0.544 & 0 & 0 & 0 & 0.544w & -1.564v \\ 0 & 1.564 & 0 & -0.544w & 0 & 0.544u \\ 0 & 0 & 0.544 & -1.564v & -0.544u & 0 \\ 0 & 0.544\ w & -1.564v & 9.94E-6 & 9.94E-6r & -1.79E-5q \\ -0.544\ w & 0 & 0.544u & -9.94E-6r & 1.76E-5 & 9.94E-6\ p \\ 1.564\ v & -0.544\ u & 0 & 1.79E-5q & -9.94E-6\ p & 9.94E-6 \end{bmatrix} \begin{bmatrix} \dot{u} \\ \dot{v} \\ \dot{w} \\ \dot{p} \\ \dot{q} \\ \dot{r} \end{bmatrix}$$

$$+ \left[K_q\right]\left[\dot{q}\left|\dot{q}\right|\right] + \left[K_L\right]\left[\dot{q}\right] = \left[F\right]$$

For our case study the model is simplified as 3 degree of freedom system (surge, heave, yaw), or (u, v, $\dot{q}$). So the equations of motion will be:

$$\begin{bmatrix} 3.739 & 0 & 0 \\ 0 & 3.739 & 0 \\ 0 & 0 & 0.154 \end{bmatrix} \begin{bmatrix} \dot{u} \\ \dot{v} \\ \dot{q} \end{bmatrix} + \begin{bmatrix} 0.544 & 0 & 0.544w \\ 0 & 1.564 & 0 \\ -0.544w & 0 & 1.76E-5 \end{bmatrix} \begin{bmatrix} \dot{u} \\ \dot{v} \\ \dot{q} \end{bmatrix} + \left[K_Q\right]\left[\dot{q}\left|\dot{q}\right|\right] + \left[K_L\right]\left[\dot{q}\right] = \left[F\right]$$

The linear and quadric hydrodynamic coefficients $\left[K_L\right]$, $\left[K_Q\right]$ are estimated experimentally or using computational fluid dynamic (CFD) models. The computational fluid dynamic model is introduced first.

IV. COMPUTATIONAL FLUID DYNAMIC MODELING

Estimation of the hydrodynamic coefficients is accomplished by creating a model for the ROV frame, which is subjected to boundary conditions as close as possible to the same conditions of the real case study.
The governing equations are set of equations solved by ANSYS CFX 12 which are the unsteady Navier-Stokes equations in their conservation form. The solution of these equations introduces the solution of the whole problem.

4.1 ROV CFD model

The ROV CFD model is created using ANSY-CFX 12. The model is composed of the ROV frame, water fluid, inlet, and outlet areas of water. The ROV frame is defined as wall, the water is defined as domain, while the inlet and outlet areas represent the inlet and outlet section of water domain. The inlet boundary condition is applied to inlet section of water domain which is defined by the velocity at inlet. The outlet boundary condition is applied to the outlet section of water domain and the atmospheric pressure is applied to the outlet boundary. The water domain length is set to be ten times the length of ROV.

4.1.1 ROV Mesh

The water (fluid) region, the inlet, outlet, and wall areas are meshed using ANSYS-CFX Mesh. The water region is meshed using tetrahedron element. The mesh is 278466 elements as shown in Fig. 3. The inlet and outlet areas are meshed using triangle element. The ROV region is meshed using triangle element. The walls region is meshed using triangle element, the walls is consists of top, bottom, front, and back.

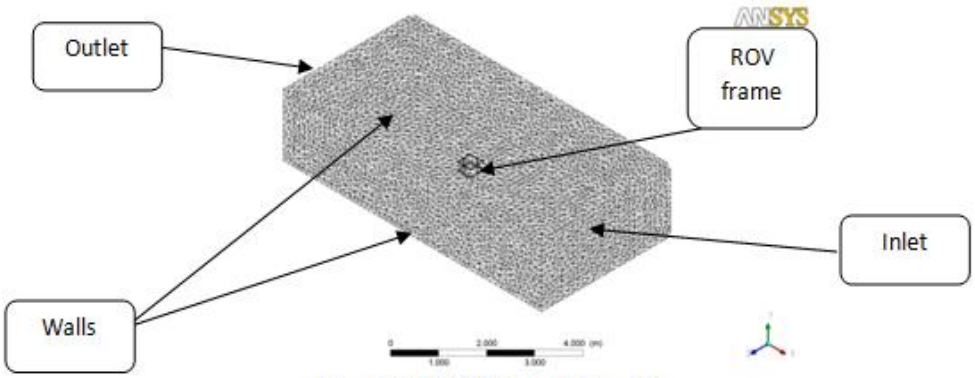

Fig. 3 ROV CFX model mesh

4.1.2 CFD Solution of the ROV in surge direction

The model is run for the evaluation of the drag force in the ROV region. Water flow is set to inlet from the inlet area, and the outlet is set to atmospheric pressure while the other 4 sides are set as walls. Fig. 4 show this configuration.

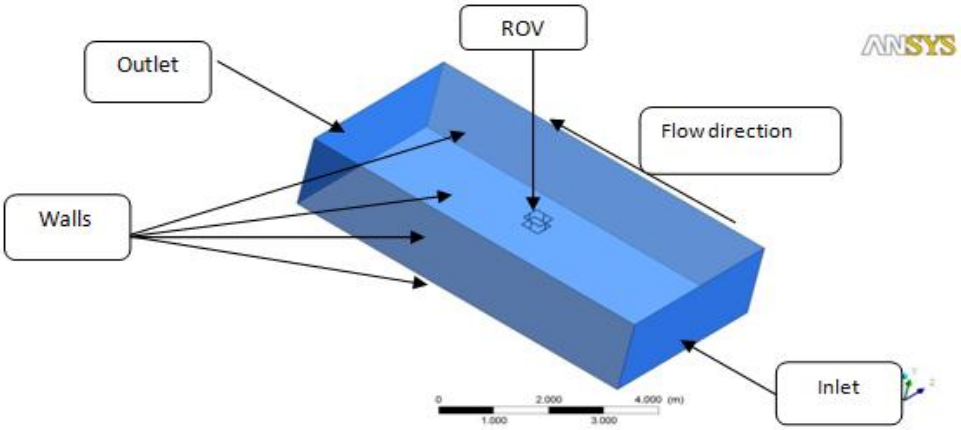

Fig. 4 CFX model for flow in surge direction

For motion in surge (x) direction the inlet velocity is varied from 0.1 m/s to 1 m/s, while the outlet is set to atmospheric pressure. The value of the drag force in the x direction is obtained as shown in Table (3).

Table 3 Drag force in surge direction

Velocity (m/s)	0.1	0.2	0.3	0.4	0.5	0.6	0.7	0.8	0.9	1
Drag Force (N)	6.204	12.416	18.636	24.864	31.1	37.344	43.596	49.856	56.124	62.40

Using the least square method the linear and quadratic damping coefficients are obtained as shown in Table (4).

Table 4 Damping coefficients in surge direction

Linear damping coefficient N/(m/s)	61.89
Quadric damping coefficient $N/(m/s)^2$	0.398

The same model is used to estimate the force in y direction by changing the inlet and the outlet direction as well as the walls region while the other 4 sides are set as walls. The top is set as inlet velocity, and bottom is set as atmospheric pressure. Fig. 5 illustrates the adaptation of the walls and boundaries to estimate the force in heave direction. The model is run for the evaluation of the drag force in the ROV region heave direction where, the inlet velocity is varied from 0.1 m/s to 1 m/s., the inlet area take the variable velocity, while the outlet is set to atmospheric pressure.. The values of the force in the y direction is written in Table 5

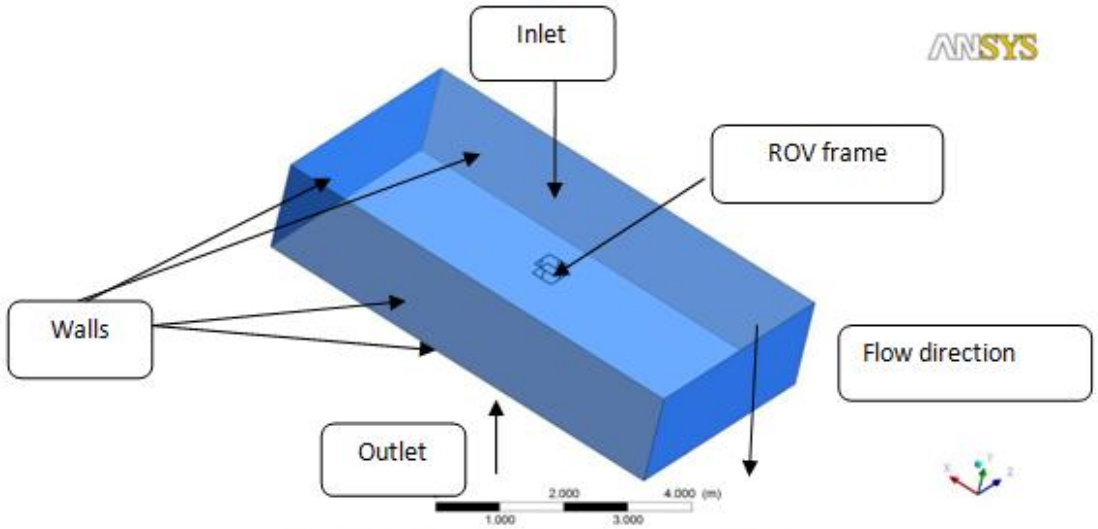

Fig. 5 CFX model for flow in heave direction.

Table 5 Drag Force in heave direction

Velocity (m/s)	0.1	0.2	0.3	0.4	0.5	0.6	0.7	0.8	0.9	1
Drag Force (N)	6.204	12.416	18.636	24.864	31.1	37.344	43.596	49.856	56.124	62.40

Using the least square method the damping coefficients is as tabulated in Table 6.

Table 6 Damping coefficients in heave direction

Linear damping coefficient N/(m/s)	61.59
Quadric damping coefficient /$(m/s)^2$	0.415

The results of the linear damping coefficients and quadric damping coefficients for both surge and heave direction are used to establish the equation of motion of the ROV frame in these directions.

V. EXPERIMENTAL WORK

Hydrodynamic coefficients are essential part of the mathematical modeling of an ROV structure model; these coefficients are estimated by experimental, analytical and computational fluid dynamics models. In this part an illustration of experimental setup, procedure and results analysis will be introduced.

5.1 Free decay pendulum motion Experiment

Estimation of hydrodynamic coefficients may obtain by several ways such as tow tank, planer motion mechanism or free decay pendulum motion. The free decay pendulum motion test is used due to its simplicity and low cost in addition to its accepted accuracy. In free decay pendulum motion the model is set to oscillate freely around its equilibrium position under the effect of its own weight and damping force only. The experimental setup is shown in Fig. 6. The model of the ROV is attached to one end of a pendulum which is a slender rod of length (40 cm). One end is equipped with a fixation to the ROV model and the other end is fixed to ball bearing to support the oscillating motion of the pendulum with minimum friction possible. In the other side of the slender rod an indicator was fixed on the roller bearing, this indicator is a short rod painted in black and marked with a white mark to improve the distinguish of the indicator from its background. Water tank with dimensions (1mx2mx1m) represent the water environment, these dimensions are selected to eliminate the effect of boundary layer formed near the tank walls. The ROV frame is fastened to the lower part of the slender rod by plastic straps to prevent any slippage of the frame. A horizontal table is used to support the digital camera parallel to the indicator rod, while the digital camera start to capture the video of the oscillating motion.

The recorded video is processed using the covariance tracking algorithm [13] to obtain the variation of angle with time digitally. These values is substituted into the next dynamic equations to obtain the hydrodynamic coefficients and added mass.

Fig. 6 Experimental set up in surge and heave direction

5.2 Dynamic Equation of Free Decay Pendulum

Consider an object of interest attached at the end of the pendulum and fully submerged in the water. The object moves in a circular path with radius(r) as shown in Fig. 7

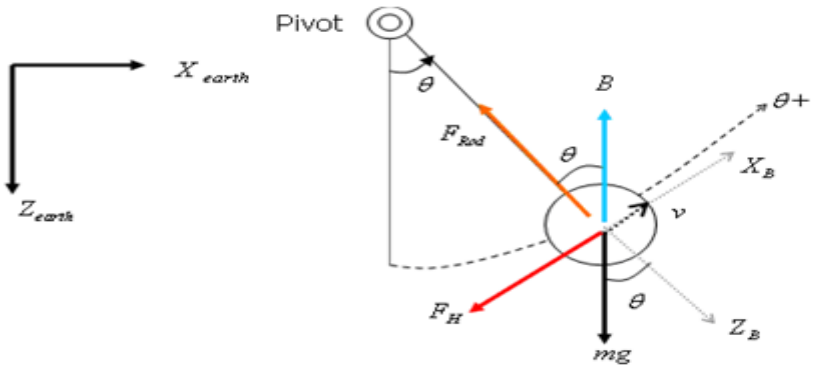

Fig. 7 Free body diagram of the pendulum under hydrodynamics forces

in the earth-fixed frame, the object is rotating about the pivot point. However, in the body-fixed frame, the object only moves in the surge direction at any instance; the object has only velocity component in surge direction.

The added mass and the damping coefficient are defined in body fixed frame such that,

$$F_H = m_a\ddot{x} + K_L\dot{x} + K_Q|\dot{x}|\dot{x} \quad (10)$$

where F_H hydrodynamic forces, m_a added mass, K_L and K_Q are linear and quadric damping coefficient respectively.

The equation of motion in the surge direction using Newton's second law of motion:

$$\sum F = M\ddot{x} \quad (11)$$

$$-Mg\sin\theta + B\sin\theta - m_a\ddot{x} - K_L\dot{x} - K_Q|\dot{x}|\dot{x} = M\ddot{x} \quad (12)$$

Rearranging equation (12) gives:

$$(B - Mg)\sin\theta - K_L\dot{x} - K_Q|\dot{x}|\dot{x} = (M + m_a)\ddot{x}$$

$$\ddot{x} = \frac{(B-Mg)}{(M+m_a)}\sin\theta - \frac{K_L}{(M+m_a)}\dot{x} - \frac{K_Q}{(M+m_a)}|\dot{x}|\dot{x} \quad (13)$$

Equation (13) is transferred into rotational motion by substituting $\dot{x} = r\dot{\theta}$ and $\ddot{x} = r\ddot{\theta}$ then $\ddot{\theta}$ is obtained as

$$\ddot{\theta} = \alpha.\sin\theta - \beta.\dot{\theta} - \gamma.\dot{\theta}|\dot{\theta}| \quad (14)$$

where $\alpha = \frac{(B-Mg)}{(M+m_a)r}$, $\beta = \frac{K_L}{(M+m_a)}$ and $\gamma = \frac{K_Q.r}{(M+m_a)}$

Using least square method to obtain the estimated α, β, γ

$$\underbrace{\begin{bmatrix} \ddot{\theta}_1 \\ \ddot{\theta}_2 \\ - \\ - \\ - \end{bmatrix}}_{y} = \underbrace{\begin{bmatrix} sin\theta_1 & \dot{\theta}_1 & \dot{\theta}_1|\dot{\theta}_1| \\ sin\theta_2 & \dot{\theta}_2 & \dot{\theta}_2|\dot{\theta}_2| \\ - & - & - \\ - & - & - \\ - & - & - \end{bmatrix}}_{H(x)} \underbrace{\begin{bmatrix} \alpha \\ \beta \\ \gamma \end{bmatrix}}_{\theta} + error \qquad (15)$$

Subscript i = 1, 2, 3…. represent the number of samples collected from the experiment

Result, $\hat{\theta}_{LS} = (H^T H)^{-1} H^T y$ (16)

where $\theta_{LS} = [\alpha \ \beta \ \gamma]^T$

By substituting the numerical values from Table (7) into equation (16) , the values of the added mass coefficient, linear damping coefficient and quadric damping coefficient are calculated as shown in Table (8). The free decay experiment is repeated thee times

Table 7 Numerical values of ROV model test

Variable	Value
M	3.739 kg
$I_{x'}$	0.097 kg. m^2
$I_{y'}$	0.154 kg. m^2
$I_{z'}$	0.097 kg. m^2
R	0.4 m
B	2.24 kg

where M is total ROV mass, $I_{x'}$, $I_{y'}$, and $I_{z'}$ are mass moment of inertia, R radius of free decay pendulum and B is buoyancy force.

Table 8 Values of added mass and hydrodynamic coefficients in surge direction

test	Added mass (kg)	Linear damping coff. (N/(m/s))	Quadric damping coff. $(N/(m/s)^2)$
1	1.73977	59.44488	0.348868
2	1.660689	62.27559	0.282417
3	1.344367	48.12204	0.365481
Average	1.581609	56.61417	0.332256

Repeating the steps for the same frame in heave direction, the hydrodynamic coefficients are obtained as shown in Table (9)

Table 9 Values of added mass and hydrodynamic coefficients in heave direction

Test	Added mass (kg)	Linear damping coff. (N/(m/s))	Quadric damping coff. $(N/(m/s)^2)$
1	2.45729	65.45486	0.4162886
2	2.35641	68.45864	0.39684756
3	2.48923	62.89923	0.425897
Average	2.43431	65.60424	0.413011

Table 10 show values of linear and quadric damping coefficient as obtained from CFD and experimental results for surge and heave direction.

Table 10 Comparison between hydrodynamic coefficients in surge and heave direction

Test	CFD		Experiment	
	surge	heave	surge	heave
Linear damping coff. (N/(m/s))	61.89	61.59	56.61417	65.60424
Quadric damping coff. $(N/(m/s)^2)$	0.398	0.415	0.332256	0.413011

The results for linear damping coefficient perform 8.51% and 6.11% differences in surge and heave directions; however for quadric damping coefficient they perform 3.63% and 0.5% difference in heave direction. It is believed that the differences in the recorded results in Table 10 are due to boundary conditions of experiments.

VI. DYNAMIC ANALYSES

To predict the motion behavior of the underwater vehicle under the effect of the thrusting force and the hydrodynamic effect of water, we should build an equation of motion describing this behavior.
Recalling equation of motion 1 and write it in surge and heave direction leads to :

$$m\,\ddot{x} + m_{added}\,\ddot{x} + k_{Ly}\,\dot{x} + k_{qy}\,\dot{x}\left|\dot{x}\right| = T_x \tag{17}$$

$$m\,\ddot{y} + m_{added}\,\ddot{y} + k_{Ly}\,\dot{y} + k_{qy}\,\dot{z}\left|\dot{z}\right| = T_y \tag{18}$$

Equations (17, 18) are non-homogeneous second order differential equations. These equations are solved numerically using the obtained hydrodynamic coefficients to get the relation between velocity and acceleration with time in surge and heave directions.

MATLAB software is used to develop a program used for solution of the above equations with thrusting force varying from 5N to 30N and the output is plot as shown in Figs (8, 9, 10, and 11).

VII. DISCUSSION

For the case study used the range of thrusting force needed to move the vehicle within the operating speed range of (0.2 to 0.5 m/s) is (5N to 30N) in surge direction, while motion in heave direction could use thrusting force less than that value, since the heave speed usually lower than surge speed.

The response of vehicle were estimated by the solution of the vehicle equation of motion; these equations have three parameters, linear damping coefficient, quadric damping coefficient and added mass, these coefficients are estimated by different ways.
Linear and quadric damping coefficients are calculated by the ANSYS CFX® and experimentally with the free decay pendulum motion, while the added mass is calculated mathematically and experimentally by free decay pendulum motion.

Figures 8 and 9 show that for certain value of thrusting force, as the time increases the velocity also increases until it reaches constant value. It is also noted that as the thrusting force increases the value of surge and heave velocity increases which is logic with the work done by Ming-Chung Fang [4].
From Figures 10 and 11 it is also found that for certain value of thrusting force, as the time increases the acceleration decreases until it reaches constant value of zero. It is also noted that as the thrusting force increases the value of surge and heave acceleration decreases which is logic with the work done by Ming-Chung Fang [4].

ANSYS CFX® give an estimation of the damping coefficients (linear and quadric), while the added mass is calculated mathematically. These values are used to substitute into the equation of motion. The relation between velocity and time were plotted and compared with the solution of the equation of motion obtained from the practical estimation as shown in Fig. 12 for surge direction and Fig 13 for heave direction.
The acceleration also is plotted for both theoretical and practical coefficients estimations as shown in Fig. 14 for surge direction, and Fig.15 for heave direction.

Figures14 and 15 shows that the initial acceleration estimated theoretically was greater than the estimated practically, that is because the main factor effected the initial acceleration is the added mass, and theoretically the added mass was calculated as if the frame was composed of tubes only and did not include tee connections and elbows, while the practical estimation considered the whole structure.

In both estimations the acceleration decays to zero with time where the drag force increases with the vehicle's velocity increases until it equals the thrusting force. Figures (12, 13, 14 and 15) shows that the vehicles response estimated practically and theoretically were similar verifying that the methods used are accurate.
For more accurate modeling, the ambient flow velocity effect on thrusting force value must be considered, since the thrusting force is assumed constant, but it varies with the vehicle speed.

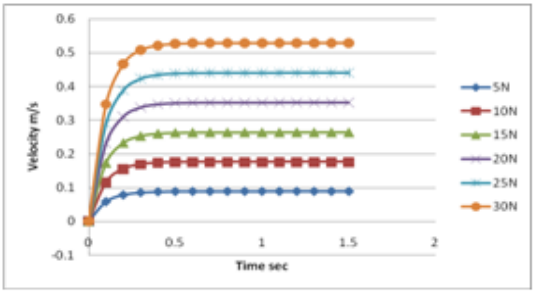

Fig. 8 Variation of velocity with time in surge direction at different thrusting force

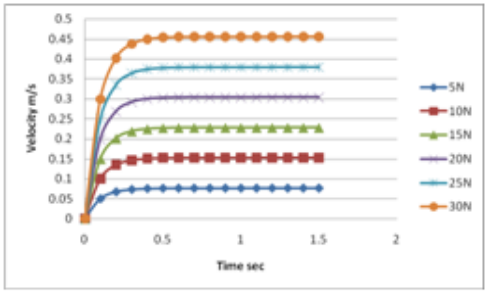

Fig.9 Variation of velocity with time in heave direction at different thrusting force

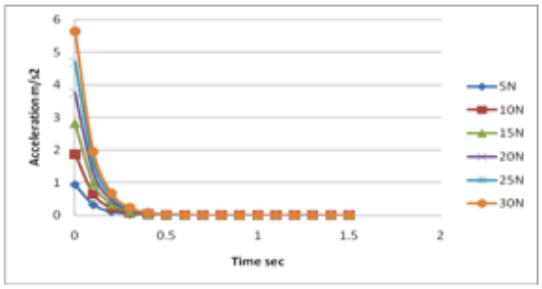

Fig.10 Variation of acceleration with time in surge direction at different thrusting force

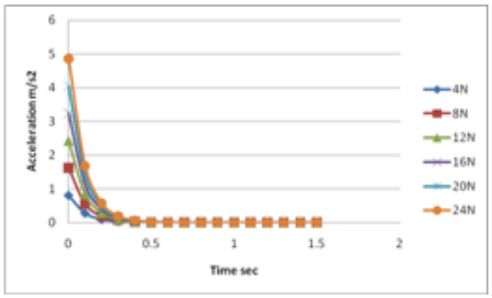

Fig. 11Variation of acceleration with time in heave direction at different thrusting force

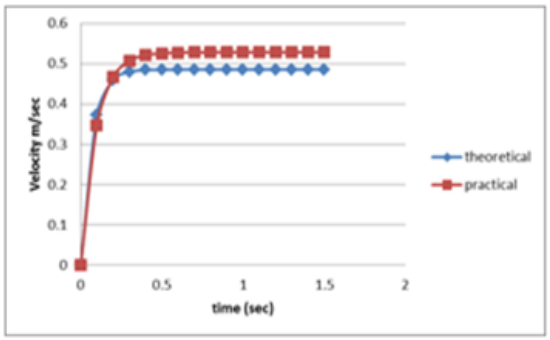

Fig.12 Comparison between variation of velocity with time in surge direction theoretically and practically

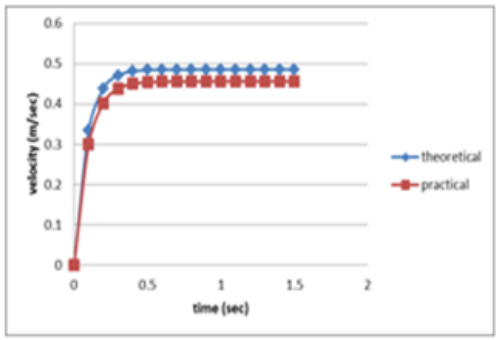

Fig. 13 Comparison between variation of velocity with time in heave direction theoretically and practically

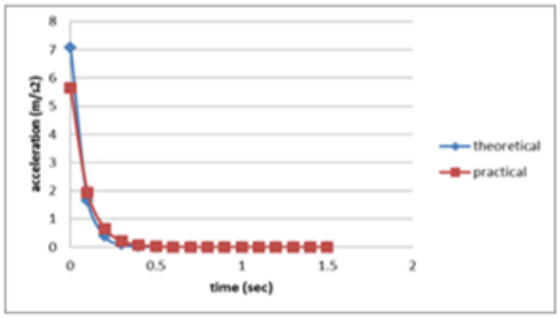

Fig. 14 Comparison between variation of acceleration with time in surge direction theoretically and practically

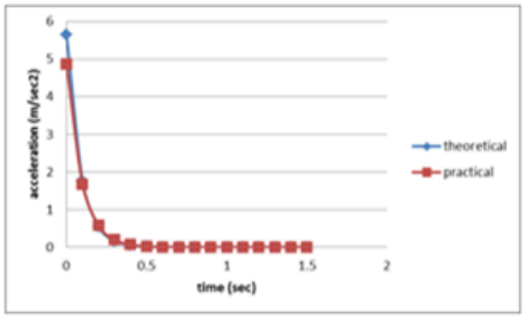

Fig. 15 Comparison between variation of acceleration with time in heave direction theoretically and practically

VIII. CONCLUSION

The equations of motion of the used ROV model include three parameters. These parameters are linear, quadratic, damping coefficient and added mass. The linear and quadric damping coefficients are obtained using the ANSYS CFX® computational fluid dynamic software and experimentally using free decay pendulum motion test. The added mass coefficient is obtained theoretically and experimentally. Comparisons show that good agreements were obtained for both results. Good agreement is achieved between the variation of velocity and acceleration with time at cretin thrusting force obtained theoretically and practically.

For more accurate modeling, the ambient flow velocity effect on thrusting force value should be calculated, since the thrusting force is assumed constant, but it varies with the vehicle speed.

Free decay pendulum motion test is suitable for simple modeling of two direction motion vehicle, but for full simulation of six degree of freedom vehicle a planner motion mechanism is preferred.

REFERENCES

[1.] F.R. Driscolla,, R.G. Lueckb, M. Nahon, "Development and validation of a lumped-mass dynamics model of a deep-sea ROV system", J of Applied Ocean Research, Vol. 22, pp. 169–182 , 2000.

[2.] B. Buckham, M. Nahon, M. Seto, X. Zhao, C. Lambert, "Dynamics and control of a towed underwater vehicle system, part I: model development", J of Ocean Engineering, Vol. 30, pp. 453–470, 2003.

[3.] J. Evans, M. Nahon, "Dynamics modeling and performance evaluation of an autonomous underwater vehicle", J of Ocean Engineering, Vol. 31, pp 1835–1858, 2004.

[4.] M. Fang, C. Hou, J. Luo, "On the motions of the underwater remotely operated vehicle with the umbilical cable effect", J of Ocean Engineering, Vol. 34, pp1275–1289, 2007.

[5.] Z. Ke-qiang, Z. Hai-yang, Z. Yu-song, G. Jie, "A multi-body space-coupled motion simulation for a deep-sea tethered remotely operated vehicle", Journal of Hydrodynamic, Vol. 20(2), pp 210-215, 2008.

[6.] J. Kim, W. K. Chung, "Accurate and practical thruster modeling for underwater vehicles", J of Ocean Engineering, Vol. 33, pp 566–586, 2006.

[7.] F. Axisa and J. Antunes, "Modeling of Mechanical Systems", J of Fluid Structure Interaction", Volume 3, pp 1-4

[8.] Peter Stevenson, Derek graham, "Advanced Materials and Their Influence on The Structural Design of AUV's" ,Technology and Applications of Autonomous Underwater Vehicle, pp 77-91.

[9.] Andrew Ross, Thor I. Fossen, Tor Arne Johansen, "Identification of Underwater Vehicle Hydrodynamic Coefficients Using Free Decay Tests", 2004.

[10.] Eng YH, Lau WS, Low E., Seet GGL and CS Chin, "Estimation of the Hydrodynamics Coefficients of an ROV using Free Decay Pendulum Motion", Engineering Letters, 16:3, EL_16_3_09, 2008.

[11.] A.H. Techet, "Hydrodynamics Readings", A. Techet , 2005.

[12.] Gianluca Antonelli, "Underwater Robots Motion and Force Control of Vehicle-Manipulator Systems", Second edition, Springer-Verlag Berlin Heidelberg, 2006.

[13.] F. Porikli and O. Tuzel. "Multi-kernel object tracking", Proceedings of IEEE Int'l. Conference on Multimedia and Expo, Amsterdam, Netherlands, 2005.